REPORT DOCUMENTATION PAGE

Form Approved
OMB No. 0704-0188

1. REPORT DATE *(DD-MM-YYYY)*	2. REPORT TYPE	3. DATES COVERED *(From - To)*
04-01-2006	Technical Paper	

4. TITLE AND SUBTITLE

A Model of Ablative Capillary Discharge (PREPRINT)

5a. CONTRACT NUMBER

5b. GRANT NUMBER

5c. PROGRAM ELEMENT NUMBER

6. AUTHOR(S)
Leonid Pekker (ERC); Jean-Luc Cambier (AFRL/PRSA)

5d. PROJECT NUMBER
23040256

5e. TASK NUMBER

5f. WORK UNIT NUMBER

7. PERFORMING ORGANIZATION NAME(S) AND ADDRESS(ES)

Air Force Research Laboratory (AFMC)
AFRL/PRSA
10 E. Saturn Blvd.
Edwards AFB CA 93524-7680

8. PERFORMING ORGANIZATION REPORT NUMBER

AFRL-PR-ED-TP-2006-013

9. SPONSORING / MONITORING AGENCY NAME(S) AND ADDRESS(ES)

Air Force Research Laboratory (AFMC)
AFRL/PRS
5 Pollux Drive
Edwards AFB CA 93524-7048

10. SPONSOR/MONITOR'S ACRONYM(S)

11. SPONSOR/MONITOR'S NUMBER(S)
AFRL-PR-ED-TP-2006-013

12. DISTRIBUTION / AVAILABILITY STATEMENT

Approved for public release; distribution unlimited (AFRL-ERS-PAS-06-019)

13. SUPPLEMENTARY NOTES
Presented at the 13th International Heat Transfer Conference (IHTC), Sydney, Australia, 13-18 Aug 2006

14. ABSTRACT

An engineering model of a steady capillary plasma discharge is presented. Two regimes of operation are studied and compared, differing by the assumptions made in the treatment of the radiative fluxes. In the first case, the plasma density is high enough that the radiation Rosseland mean free path is smaller than the capillary radius; this case of black-body radiation leads to super-high pressures. In the second case, the radiation mean free path is larger than the capillary length, and the limit of volume radiation is achieved, leading to more moderate pressures. Both assumptions lead to different scaling laws, with consequences for the capillary design. The current model is based on the conservation laws for mass, momentum and energy, and assumes local thermodynamic equilibrium (LTE) and sonic conditions at the exit plane. Various assumptions have been made in the literature about the amount of heat being used for the phase change and the ionization cost of the wall material, and the effect of these assumptions is also examined. Finally, we discuss a number of potential applications of the discharge, describe planned experiments, and discuss on-going work in extending the model to multi-dimensions and the intermediate (between black-body and volume radiation) regime.

15. SUBJECT TERMS

16. SECURITY CLASSIFICATION OF:			17. LIMITATION OF ABSTRACT	18. NUMBER OF PAGES	19a. NAME OF RESPONSIBLE PERSON
a. REPORT	b. ABSTRACT	c. THIS PAGE			Dr. Jean-Luc J. Cambier
Unclassified	**Unclassified**	**Unclassified**	A	13	19b. TELEPHONE NUMBER *(include area code)* N/A

Standard Form 298 (Rev. 8-98)
Prescribed by ANSI Std. 239.18

A MODEL OF ABLATIVE CAPILLARY DISCHARGE (PREPRINT)

L. Pekker[1], J.-L. Cambier[2]
[1]ERC Inc., Edwards AFB, CA 93524, USA
[2]Air Force Research Laboratory, Edwards AFB, CA 93524.

Abstract

An engineering model of a steady capillary plasma discharge is presented. Two regimes of operation are studied and compared, differing by the assumptions made in the treatment of the radiative fluxes. In the first case, the plasma density is high enough that the radiation Rosseland mean free path is smaller than the capillary radius; this case of black-body radiation leads to super-high pressures. In the second case, the radiation mean free path is larger than the capillary length, and the limit of volume radiation is achieved, leading to more moderate pressures. Both assumptions lead to different scaling laws, with consequences for the capillary design. The current model is based on the conservation laws for mass, momentum and energy, and assumes local thermodynamic equilibrium (LTE) and sonic conditions at the exit plane. Various assumptions have been made in the literature about the amount of heat being used for the phase change and the ionization cost of the wall material, and the effect of these assumptions is also examined. Finally, we discuss a number of potential applications of the discharge, describe planned experiments, and discuss on-going work in extending the model to multi-dimensions and the intermediate (between black-body and volume radiation) regime.

1 Introduction

The capillary discharge has been previously studied as potential electro-thermal and electro-thermo-chemical guns device by various investigators since the mid 1980s, e.g. Tidman et al. (1986), Loeb and Kaplan (1989), Powell and Zielinski (1992), Zoler et al. (1994, 1995), Gilligan and Mohanti (1990), and Shafir et al. (2005). These studies investigated the dynamics of high-pressure ablative plasma discharges achieved through the dissipation of high (several kA) current pulses in a narrow channel. Other types of capillary discharges operating with much faster pulses and at lower pressure have more recently been the subject of increased attention as potential devices for X-ray lasers, wakefield acceleration and ultra-intense laser guiding (e.g., Cros et al., 2000). Therefore, the capillary discharge can operate at least in two regimes; as a very high-pressure, ablative plasma discharge and a low-pressure, non-ablative fast-pulse discharge. The intermediate regime has not been thoroughly explored, but is also of potential interest for propulsive or other applications with a high duty cycle. The high-pressure, low-temperature regime – of the order of Giga-Pascal (GPa) and 1-3 eV respectively – is a result of fast ablation of the capillary walls, and presents formidable challenges for re-usability, due to the very high stresses. The low-pressure, high electron temperature – of the order of Mega-Pascal (MPa) and 100 eV – regime is more amenable to repeated use, but has a reduced thrust or acceleration performance, and thermal non-equilibrium effects can be significant. Ideally the intermediate pressure and temperature regime, typically of the order of 5-15 MPa and 4-10 eV, could be handled with current material strength, and reduced ablation rates could allow continuous or repeated feedstock injection (propellant). This approach was considered by Burton et al. (1990, 1991) for the design and testing of a prototype Pulsed Electrothermal Thruster (PET) operating at

30-50 MPa and 2 eV, yielding a thrust-to-power ratio $T/P \approx 70\,mN/kW$ with water injection, a very respectable figure of merit for high-power electric propulsion (EP) systems. The current study is partially motivated by the need to further explore this intermediate pressure regime and the need to better evaluate and optimize device performance for applications of interest. For example, the pressure and temperature (P,T) conditions mentioned above could potentially lead to a thrust density of at least 10 MN/m^2 if operated continuously and a specific impulse of 3,000 sec; this corresponds to a thrust of approximately 1 kN per capillary, an impressive potential for a plasma thruster device. Capillaries can be combined together, improving the thrust/mass ratio, but the actual performance would probably be limited by the duty cycle than can be practically maintained. Continuous or high-frequency operation may be difficult, due to the high rates of energy deposition and heat transfer in a small volume; therefore, predictive analysis of the thermodynamics of the discharge is an essential first step in the development of this device. For this purpose, we have developed a zero-dimensional (0D) model of the discharge to derive scaling laws and global properties of plasma capillary thrusters; this model will be further expanded to one- and two-dimensional models, currently under development, with additional physics and unsteady effects.

2 Description of the Model

2.1 Conservation Laws and Approximations

The ablative capillary discharge can be approximately described by a three-layer configuration. The outer-most layer is the solid wall, usually some form of polyethylene, occasionally Teflon or some other insulating material, which evaporates and enters the transition, or "boundary" layer, where it can be dissociated, ionized and heated. The innermost layer is the plasma core, usually considered fully ionized and uniform. Electrodes are located at both end, with one being open-ended, through which the plasma can expand. A current pulse of several kA – from 2 kA to 140 kA in some cases – and of milli-second duration – from 0.1 to 5 ms in the ablative case – flows through the plasma along the capillary. The large Ohmic heating is responsible for rapid temperature rise, ionization, ablation, and radiation.

The first zero-dimensional analytical model of ablative capillary discharges was developed by Loeb and Kaplan (1989); using a number of simplifying assumptions, these authors obtained scaling laws for the plasma temperature, pressure, wall ablation rate, and other parameters of the capillary discharge as function of the current, radius (R_c) and length (L_c) of the capillary, a significant progress the time. In later works – see for example Powell and Zielinski (1992) – the Saha equation was used to more accurately calculate the plasma composition and enthalpy of the capillary discharge. The most important assumptions made relate to the amount of radiation emitted, as well as the amount used for ablation and phase change. In a 0D model, the conservation laws for mass and energy can be expressed as:

$$\frac{d\rho}{dt} = \dot{\rho}_a + \dot{\rho}_e \tag{1a}$$

$$\frac{d}{dt}(\rho\breve{\varepsilon}) = \eta \cdot j^2 + \dot{\rho}_e \breve{h}_e - \frac{2}{R_c} q_r\big|_{Rc} + \dot{\rho}_a \breve{h}_a \tag{1b}$$

where $\dot{\rho}_a, \dot{\rho}_e$ are respectively the rates of mass addition by ablation and removal by flow at the exit, per unit volume. Correspondingly, the mass injection and removal ($\dot{\rho}_a > 0, \dot{\rho}_e < 0$) introduce source terms for the total energy in equation (1b). Here, we

use the following notation: the specific (per unit mass) thermal energy and enthalpy are $\varepsilon = C_v T / \overline{m}$, $h = C_p T / \overline{m}$, while total energy and enthalpy include kinetic and internal energies:

$$\breve{\varepsilon} = (\gamma - 1)^{-1} kT / \overline{m} + \tfrac{1}{2}\vec{u}^2 + \Delta\tilde{\varepsilon}_V + \Delta\tilde{\varepsilon}_D + \Delta\tilde{\varepsilon}_X + \Delta\tilde{\varepsilon}_I \qquad (2)$$

and similarly for the total enthalpy ($\breve{h} = \breve{\varepsilon} + kT/\overline{m}$). In (2) we have expressed the specific heat at constant volume, and described the total internal energy as changes due to vaporization (V), dissociation (D), electronic excitation (X) and ionization (I). If the plasma was comprised on molecular species, vibrational and rotational excitation should also be included; however, the conditions are such that complete dissociation can be assumed, and multi-stage ionization and electronic excitation make the bulk of the internal, or phase-change energy $\Delta\varepsilon_\Phi$. The first term on the RHS of equation (1b) is the Ohmic heating, and is determined by the plasma conditions, i.e. the resistivity η. The third term is the radiation flux at the edge ($r = R_c$) of the plasma column. Prior capillary models have used various assumptions to relate the mass and enthalpy flows from the ablated material with the radiation flux. For example in the time-dependent 0D-model of Gilligan and Mohanti (1990), the ablated material from the transition layer is <u>not</u> dissociated or ionized before entering into the plasma, and therefore the rate of ablation is determined by: $\dot{\rho}_a \Delta\varepsilon_V = (2/R_c) \cdot q_r\big|_{R_c}$, since the radiation only performs the work of vaporizing the material. Gilligan and Mohanti also assumed the thermal radiation q_r incident on the insulator surface to be a fraction *f* (the grey factor) of the blackbody radiation leaving the plasma, $q_r = f \cdot \sigma_{SB} T^4$. Assuming local thermodynamic equilibrium (LTE) and using the Saha-Boltzmann equation, Gilligan and Mohanti calculate the internal energy of the plasma, the resistivity and other thermodynamic parameters. To get an agreement with experiments showing very small smaller ablation rate, they must assume that only a small fraction ($f \ll 1$) of the radiation is absorbed in the wall. This model differs notably from that of Loeb and Kaplan by the assumptions made in the amount of radiant energy absorbed, and the "work" done by this radiation. This will be further discussed hereafter.

The 0D model that is considered here is similar to prior work, can be also described by equations (1a-b), and also uses some key approximations. In all cases considered here, the ratio of plasma pressure to magnetic pressure β is always large and MHD effects can be neglected. Viscous effects and species diffusion can also be neglected, due to the high flow Reynolds number, typically of the order of 10^6. Thermal equilibrium is obtained between electrons and heavy particles, i.e. $T_e \approx T_h$; this is characterized by the LTE factor, the ratio of the thermal energy exchange rate between electrons and heavy particles to the electron Ohmic heating rate, which for the conditions of interest is typically $10 - 10^3$.

2.2 Physical Model

The electrical conductivity plays a key role in the model, by determining the rate of Joule heating. Neglecting the induced magnetic field, the conductivity is given by:

$$\sigma = \frac{n_e e^2}{m_e(\nu_{ei} + \nu_{en})} \qquad (3)$$

The electron-neutral collision frequency is:

$$\nu_{en} = n_e \sum_s < \sigma_m^{e,s} v_e > \approx n_e \bar{v}_e \sum_s < \sigma_m^{e,s} > \tag{4}$$

with $\bar{v}_e$ the mean electron thermal speed and $\sigma_m^{e,s}$ the collision cross-sections for momentum (m) exchange with species s; these are taken from Powell and Zielinski:

$$\bar{\sigma}_{eC} \approx 30\pi a_0^2 \approx 2.64\times10^{-19} \quad [\mathrm{m}^2] \tag{5a}$$

$$\bar{\sigma}_{eH} \approx 17\pi a_0^2 \approx 1.49\times10^{-19} \quad [\mathrm{m}^2] \tag{5b}$$

where $a_0 = 4\pi\varepsilon_o\hbar^2/m_e e^2 \approx 5.29\times10^{-11}$ [m] is the classical Bohr radius. The electron-ion collision cross-section is defined by the Spitzer equation (Spitzer and Härm, 1953):

$$\nu_{ei} = \frac{38\,\bar{Z}\,n_e e^2}{\gamma_e \cdot m_e T^{3/2}} \cdot \ln\bar{\Lambda} \tag{6}$$

The factor $\gamma_e(\bar{Z})$ in equation (6) is a weak function of $\bar{Z}$ and can be approximated as: $\gamma_e \approx 0.58 + 0.1\cdot(\bar{Z} - 1)$. The thermally-averaged Coulomb logarithm $\ln\bar{\Lambda}$ can be approximated as: $\ln\bar{\Lambda} \approx 24.38 + 1.5\ln T_{[\mathrm{eV}]} - 0.5\ln n_{[\mathrm{cm}^{-3}]}$. For a fully-ionized gas, the (Spitzer) conductivity can be written as:

$$\sigma = \frac{\beta}{\bar{Z}} \frac{T_{[\mathrm{K}]}^{3/2}}{\ln\bar{\Lambda}} \quad \text{with} \quad \beta \approx 1.07\times10^{-2} \tag{7}$$

While Loeb and Kaplan introduce a temperature and density-dependent β in order to use (7) for non fully-ionized plasmas as well, we keep equation (3) for the general case, and use expression (7) for the fully-ionized case only, which will be useful when considering the scaling laws for a simplified model.

The plasma will be considered either fully-ionized or in chemical equilibrium. In the latter case, the electronic partition of bound levels is also included. We consider 13, 12, and 11 pseudo-levels – groups of elementary levels with combined statistical degeneracy and averaged energy – for C_I, C_{II} and C_{III}, i.e. neutral, 1st-ionized and second-ionized Carbon atoms; Hydrogen (H_I) is modeled by 6 pseudo-levels. The Saha equilibrium function is given by:

$$S_{m+1}(T) = \frac{n_{m+1}\cdot n_e}{n_m} = A\cdot T^{3/2} \cdot \frac{u_{m+1}}{u_m} \cdot e^{-\frac{I_{Cm}}{kT}} \tag{8}$$

with $A = 6.04\times10^{27}$ $[m^{-3}eV^{-3/2}]$ and u_m the electronic partition function:

$$u_m = g_m^0 + g_m^1 \cdot e^{-\frac{\Delta E_{1(m)}}{kT}} + g_m^2 \cdot e^{-\frac{\Delta E_{2(m)}}{kT}} + \ldots.. \tag{9}$$

One can then express the ion densities as function of total species density and the equilibrium constants. For Carbon,

$$n_{m(C)} = n_C \cdot \frac{\prod_{p>1}^{p\le m}(n_e^{-p} S_p^{(C)})}{1 + \prod_{p>0}(n_e^{-p} S_p^{(C)})} \tag{10}$$

where m indicates the ionization stage. These expressions are similar to equation (17) of Powell and Zielinsky. Equations for Hydrogen are obtained similarly, with the exception of having only one ionized state. Using charge neutrality the electron density can be written as:

$$n_e = \sum_s n_s \sum_{m(s)} m \cdot \frac{\prod_{p\ge1}^{p\le m}(p\cdot n_e^{-p} S_p^{(C)})}{1 + \prod_{p>0}(n_e^{-p} S_p^{(C)})} \tag{11}$$

Solving this non-linear equation for the electron density as function of the temperature will allow us to determine all atom and ion concentrations.

The plasma is also considered weakly non-ideal, with the main effect being a lowering of the ionization potential and pressure from the ideal plasma conditions. Thus, in the model by Griem (1962), $I_m = I_m^{ideal} - \Delta I(n,T)$ and $P = nkT - \Delta P(n,T)$, with:

$$\Delta I_m = \frac{me^2}{4\pi\varepsilon_o \lambda_{De}} \approx \frac{7.75\times10^{-4}}{(T_{[\mathrm{eV}]})^{1/2}} \cdot \left(\frac{n_e}{10^{20}[\mathrm{m}^{-3}]}\right)^{1/2} \ [\mathrm{eV}] \qquad (12a)$$

$$\Delta P = \frac{kT}{24\pi\lambda_{De}^3} \approx \frac{3.30\times10^{-3}}{(T_{[\mathrm{eV}]})^{1/2}} \cdot \left(\frac{n_e}{10^{20}[\mathrm{m}^{-3}]}\right)^{3/2} \ [\mathrm{Pa}] \qquad (12b)$$

where λ_{De} is the Debye length. We expect the lowering to be as large as $\Delta I_0 \approx 1.15$ eV and $\Delta P \approx 2$ MPa for the discharge conditions considered here, i.e. up to 10% effect.

2.3 Model Formulation

We consider two classes of discharges: 1) a high pressure/optically thick case, where the average (Rosseland) radiation m.f.p. is much smaller than the capillary radius and the plasma radiation can be modeled by a blackbody; 2) a low-pressure/optically thin case, where the radiation m.f.p. is larger than the characteristic dimensions and the plasma radiation is given by volumetric radiative emission. These assumptions are limiting cases of a more complex radiation transfer model required for a more detailed evaluation of the radiative flux absorbed by the transition layer and the capillary wall; this detailed model is currently under development and will be described in the future, while the current approximate model provides preliminary estimates of the heat transfer regime and bounding limits.

The first version of our 0D model is similar to Loeb & Kaplan. In this model, the plasma radiation ablates, vaporizes, ionizes and heats the ablative gas in the transition layer up to plasma conditions. Also, it is assumed that the average energy cost per ion, that includes the vaporization, dissociation and ionization energies, is a fixed constant, and all carbon ions are twice ionized. According to this model, $\dot{\rho}_a \breve{h}_a = 2q^{rad}/R_c$, and the enthalpy injection and radiative losses cancel each other out in the energy conservation equation (1b). The surface-integrated fluxes are then defined for the black-body (BB) and volumetric radiation (VR) cases:

– Optically-thick (BB) case: $F_{BB} = (2\pi R_c L)\cdot\sigma_{SB}T^4$ (13a)

– Optically-thin (VR) case: $F_{VR} = (\pi R_c^2 L)\cdot\sigma_{VR}(\overline{Z}\,\overline{Z^2})\cdot n_i^2 T^{1/2}$ (13b)

where in SI units, $\sigma_{VR} \approx 1.42\times10^{-40}$. The volumetric radiation in (13b) is assumed to be due to continuous emission (bremsstrahlung), assuming that all line radiations (including bound-free transitions) are self-trapped. This model simplifies the scaling analysis, while the free-bound emission will be added later. The *Z*-factors in (13b) originate from a factor $\sum_k n_e n_k Z_k^2$ in the expression of the bremsstrahlung radiation, where the summation runs over all ion species.

Neglecting the kinetic energy, the total enthalpy of the ablated flow is:

$$\breve{h}_a \approx \overline{M}_a^{-1}\left[\Delta\varepsilon_\Phi + C_p(1+\overline{Z})(\alpha_C+\alpha_H)\cdot kT\right] \qquad (14)$$

Here, α_C and α_H are the numbers of carbon and hydrogen atoms in the "polyethylene molecule" of mass $\overline{M}_a = (\alpha_C A_C + \alpha_H A_H) \cdot M_{amu}$ (in SI units), M_{amu} is the atomic mass unit and $C_p = \gamma/(\gamma - 1)$ is the specific heat at constant-pressure, with $\gamma = 5/3$. As in equation (2), $\Delta\varepsilon_\Phi$ includes the energies of dissociation, electronic excitation and ionization. Using the formation energies of the atoms and molecules in various phases, one can construct the chain of internal energy changes for each ablating molecule as (for simplicity we include the electronic excitation into ionization):

$$\begin{aligned}\Delta\varepsilon_\Phi &= \left[\Delta\varepsilon_V\right] + \left[\Delta\varepsilon_D\right] + \left[\Delta\varepsilon_{X-I}\right] \\ &= \left[\varepsilon^o_{CH(g)} - \varepsilon^o_{CH(s)}\right] + \left[\alpha_C \varepsilon^o_C + \alpha_H \varepsilon^o_H - \varepsilon^o_{CH(g)}\right] + \left[\alpha_C (\varepsilon^o_{C^{++}} - \varepsilon^o_C) + \alpha_H (\varepsilon^o_{H^+} - \varepsilon^o_H)\right] \\ &= \alpha_C \varepsilon^o_{C^{++}} + \alpha_H \varepsilon^o_{H^+} - \varepsilon^o_{CH(s)} \approx \alpha_C \varepsilon^o_{C^{++}} + \alpha_H \varepsilon^o_{H^+}\end{aligned} \quad (15)$$

Defining an average formation energy of ions as:

$$u_\Phi = \frac{\alpha_C \varepsilon^o_{C^{++}} + \alpha_H \varepsilon^o_{H^+}}{\alpha_C + \alpha_H} \quad (16)$$

we can now write (14) as:

$$h_a \approx (\alpha_C + \alpha_H)\left[u_\Phi + (1 + \overline{Z}) C_p kT\right] \quad (17)$$

The inflow of material can be written as:

$$V \cdot \dot{\rho}_a = \frac{F^{rad}}{\breve{h}_a} \approx \overline{M}_a \frac{F^{rad}}{h_a} \quad (18)$$

with F^{rad} taking one or the other form described in (13a-b). Defining the ion-acoustic speed in the plasma as:

$$c(T) = \left((1 + \overline{Z}) \cdot \gamma kT / M_i\right)^{1/2} \quad (19)$$

where $\overline{M}_i = \overline{A} M_{amu}$ is the average ion mass, the outflow through the open end of the capillary can be described by:

$$V \cdot \dot{\rho}_e = -(\pi R_c^2) \cdot c_1 n_1 \cdot \overline{M}_i \quad (20)$$

where $c_1 = c(T_1)$, and the suffix "1" denotes conditions at the exit plane, where sonic conditions are assumed. In the quasi steady-state, the rate of mass injection by ablation is approximately equal to the outflow rate ($\dot{\rho}_a + \dot{\rho}_e \approx 0$). Substituting the plasma radiation fluxes from (13), and using the isentropic flow relations we obtain:

$$\overline{M}_a \frac{(2\pi R_c L) \cdot (\sigma_{SB} T^4)}{h_a} = \overline{M}_i (\pi R_c^2) \cdot n_0 \cdot \Gamma \cdot c(T_0) \quad (21a)$$

$$\overline{M}_a \frac{(\pi R_c^2 L) \cdot (\sigma_{VR} (\overline{Z}\,\overline{Z^2}) \alpha_i^2 n_0^2 T_0^{1/2})}{h_a} = \overline{M}_i (\pi R_c^2)\, n_0 \cdot \Gamma \cdot c(T_0) \quad (21b)$$

where:

$$\Gamma = \left(\frac{2}{\gamma + 1}\right)^{\frac{(\gamma+1)}{2(\gamma-1)}} \quad (22)$$

the suffix "0" stands for stagnation conditions, $\alpha_i = n_i / n_h$ is the ion fraction. The volume-averaged conditions can be approximated by the stagnation conditions in the limit of a long capillary; in that case, the suffix "0" is dropped and replaced by "BB" and "VR" for the two limiting radiation models being considered. Assuming a fully ionized plasma ($\alpha_i \equiv 1$), equations (21a-b) can then be inverted to yield the ion density as function of temperature:

$$n_{BB} = \Gamma^{-1} \cdot \frac{2L}{R_c} \cdot c_{ref}^{-1} \cdot \frac{(\sigma_{SB} T^4)}{\left[u_\Phi + (1+\bar{Z}) C_p kT\right]} \cdot \left(\frac{T}{T_{ref}}\right)^{-1/2} \quad (23a)$$

$$n_{VR} = \Gamma \cdot \frac{1}{L} \cdot c_{ref} \frac{\left[u_\Phi + (1+\bar{Z}) C_p kT\right]}{(\sigma_{VR} (\bar{Z}\,\overline{Z^2}) T^{1/2})} \cdot \left(\frac{T}{T_{ref}}\right)^{1/2} \quad (23b)$$

where T_{ref} is a reference temperature (e.g. 1 eV) and $c_{ref} = c(T_{ref})$. In the energy equation (2b), and since it was assumed that $\dot{\rho}_a \breve{h}_a = 2q^{rad}/R_c$, the quasi steady-state implies that the Joule heating balances the enthalpy outflow at the open end, $(\pi R_c^2) c_1 n_1 \breve{h}_i$. Since the flow is isentropic, $\breve{h}_i$ is also the stagnation enthalpy and therefore the total heat outflow is:

$$F_{out}^E = (\pi R_c^2) \Gamma c_{ref} \left(\frac{T}{T_{ref}}\right)^{1/2} n_i \cdot \left[u_\Phi + (1+\bar{Z}) C_p kT\right] \quad (24)$$

The total energy deposition by Ohmic heating is:

$$\dot{Q} = \frac{L}{(\pi R_c^2)} \frac{I^2}{\sigma} \quad (25)$$

with I the current, and σ the conductivity (3). The energy balance ($\dot{Q} = F_{out}^E$) yields another expression for the average ion density in the discharge:

$$n_i = \frac{L \cdot I^2}{\pi^2 R_c^4} \frac{Z_{eff}^2}{\bar{Z}} \frac{\ln \bar{\Lambda}}{\beta T^{3/2}} \Gamma^{-1} c_{ref}^{-1} \left(\frac{T}{T_{ref}}\right)^{-1/2} \left[u_\Phi + (1+\bar{Z}) C_p kT\right]^{-1} \quad (26)$$

This expression is independent of the assumption made about the Rosseland radiation m.f.p. and can be applied to both cases; equality of (23a-b) and (26) yields:

$$I_{BB} = R_c^{3/2} \left(\frac{2\pi^2 \bar{Z}}{Z_{eff}^2} \beta \sigma_{SB}\right)^{1/2} \left(\frac{T^{11/2}}{\ln \bar{\Lambda}}\right)^{1/2} \quad (27a)$$

$$I_{VR} = \frac{R_c^2}{L} \Gamma c_{ref} \left(\frac{T}{T_{ref}}\right)^{\frac{1}{2}} \left(\frac{\beta \pi^2}{\sigma_{VR} (\bar{Z}\,\overline{Z^2})}\right)^{\frac{1}{2}} \left(\frac{T}{\ln \bar{\Lambda}}\right)^{\frac{1}{2}} \left[u_\Phi + (1+\bar{Z}) C_p kT\right] \quad (27b)$$

For each limiting case of optical thickness, there is a system of two equations (e.g., 23a and 27a) with two unknowns (n_i and T), given the total discharge current, which can be solved iteratively. Alternative solutions for the pressure are obtained using the assumed equation of state (EOS): $p = (1+\bar{Z}) n_i kT$.

3 Results

3.1 Scaling Laws

Scaling laws can be extracted from the formulas (23) and (27); by also ignoring the u_Φ term in these equations, it is possible to obtain simple relationships, i.e.:

– BB case: $T \propto (R_c^{-6/11}) \cdot I^{4/11}$ $P \propto (L R_c^{-32/11}) \cdot I^{14/11}$ $n \propto (L R_c^{26/11}) \cdot I^{10/11}$ (28a)

– VR case: $T \propto (L^{1/4} R_c^{1/2}) \cdot I^{1/4}$ $P \propto (L^{-1/2} R_c^{-1}) \cdot I^{1/2}$ $n \propto (L^{3/4}) I^{1/4}$ (28b)

The geometrical scaling laws are identified by the terms in parentheses, and were easily verified. The approximate scaling between temperature, current and pressure obtained from equations (23) and (27) could also be verified: in the BB case, and

assuming a constant $u_\Phi \approx 20\,\text{eV}$, the profiles of Figure 1 are obtained. At high temperature, u_Φ can be neglected and the scaling is consistent with the Loeb & Kaplan approximation given by equations (28a-b), in which case $P \propto T^{3.5}$. At low temperature ($T \ll 2\,\text{eV}$), u_Φ dominates and the pressure scaling changes: $P \propto T^{4.5}$. For the VR case, the scaling changes from $P \propto T, I \propto T$ at low temperature to $P \propto T^2, I \propto T^2$ at high temperature, neglecting the Coulomb logarithm variation.

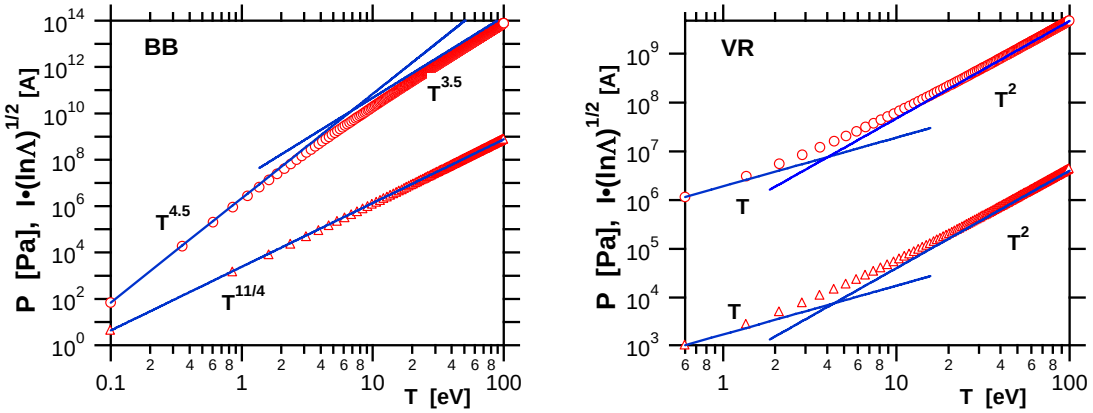

Figure 1: Scaling of pressure and current (renormalized by the Coulomb logarithm) with respect to temperature; BB and VR models, fixed u_Φ.

3.2 Equilibrium Model

In version 2 of the 0D model, the thermodynamic equilibrium formulation is used. In that case, the plasma composition and the phase change energy u_Φ are computed for each value of the temperature, though a sequence of iterations. The mass ablation rate is obtained as function of the radiative flux, and therefore the plasma temperature; given a mass ablation rate and a mass outflow rate, the plasma density itself changes until convergence is obtained. Since the plasma density is itself a function of the temperature, only the plasma temperature is required to obtain the final plasma conditions, for either model of radiative flux. The phase change energy can be compared to the constant values assumed in the version 1 of the model; the impact of the exact value of u_Φ is noticeable mostly at low (≤ 2 eV) temperature. The pressure and current in the optically thick (BB) and thin (VR) regimes could then be recomputed, and the scaling laws (23) and (27) could be recovered in the limit of high-temperature, but not at low temperature. This is expected, since the simplified (version 1) model assumed a fully-ionized plasma with twice-ionized Carbon atoms; calculations indicate that below 4 eV, this assumption starts to break down.

In fact, there is also a threshold below which no solution can be found in the optically-thin regime. This is best observed by considering equation (21b): at a given temperature, and for the thermodynamic equilibrium conditions, one cannot generally assume that the ionization fraction is unity. Therefore, the LHS of (21b) – which describes the incoming energy flux – varies as n_i^2, while the RHS – which describes the outgoing flow – varies as n_h. For a low-temperature plasma, the ion density is determined by the Saha formula, in which case $n_i^2 \propto n_h$ and both energy flows are linear functions of the density. For a fully-ionized plasma, the Saha equation is saturated, $n_i \approx n_h$ and the point of equilibrium would be obtained at the point of intersection between a parabola and a straight line, when both flows are plotted as

function of n_h. Depending on the location of the point of inflexion for the incoming mass flux, there may not be an intersection between the two curves. This can be demonstrated by plotting the two energy flows as function of the total density, for two cases of temperature. As shown in Figure 2, there is no intersection for 1 eV, and therefore no possible solution. Figure 2 shows the switch in the inflow curves between the n_h^2 scaling at low density (which favors full ionization) and the n_h scaling at high density (which favors partial ionization). There is a shift in the energy outflow profile, as expected (lines with no symbols), but it is hardly noticeable on this scale.

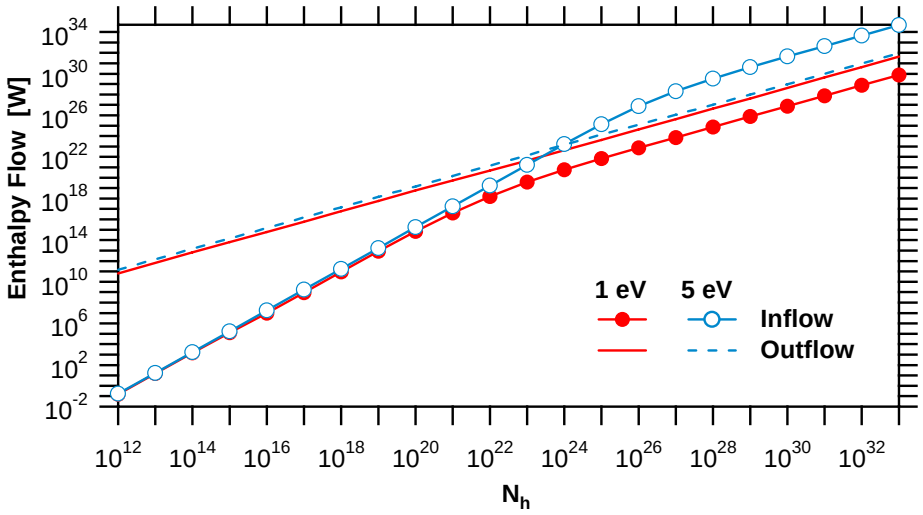

Figure 2: Incoming and outgoing total enthalpy flows for two temperatures and VR model, as function of total density.

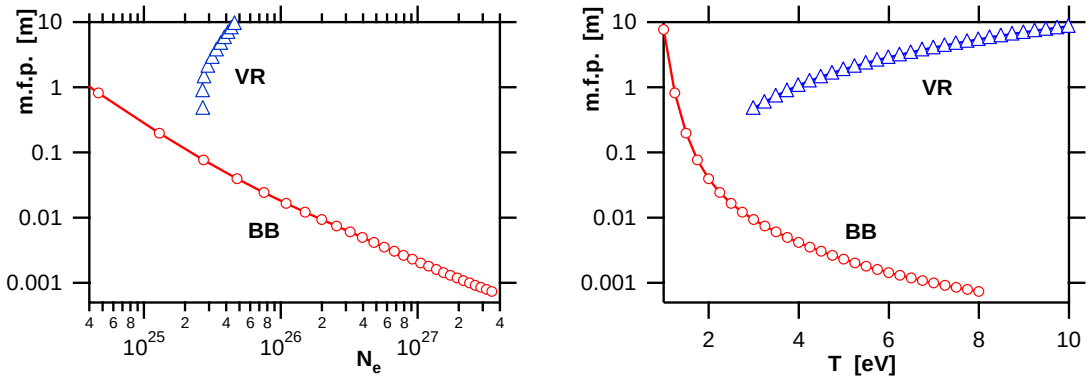

Figure 3: Rosseland mean-free-path versus (a) electron density and (b) plasma temperature.

3.3 Results and Conclusions

In the absence of a full spectral radiation transport model, the validity of each radiation model considered so far can be estimated by evaluating the Rosseland mean-free-path of the radiation, λ_R. As shown in Figure 3 for the black-body model, the condition of an optically-thick plasma ($\lambda_R \ll R_c$, with $R_c \approx 1\text{mm}$) is satisfied only at the highest values of density and temperature; this leads to extremely high pressures, of the order of 10 GPa (100,000 atm). In the VR case, the computed plasma density is confined within a much narrower range, and the mean-free-path behavior is significantly different. In that case, the optically-thin condition ($\lambda_R > L_c >> R_c$, with $L_c \approx 10\,\text{cm}$) is satisfied even at the lowest temperatures of interest. The true physical condition may be somewhere in-between, and this will be investigated in the near-future with a more detailed radiation transport model, currently under-development.

The model of volumetric radiation considered so far – see equation (13b) – accounts only for the free-free emission. Free-bound emission can also be included using a well-known approximation (Zeldovich and Raizer, 2002). The modified rate of emission now reads:

$$F_{VR} = (\pi R_c^2 L) \cdot \sigma_{VR} (\bar{Z}\,\overline{Z^2}) \cdot n_i^2 T^{1/2} \cdot \left(1 + 2\frac{\bar{I}}{T}\right) \tag{29}$$

As shown in Figure 4, for the same temperature range the enhanced emission given by equation (28) leads to lower plasma densities, as well as lower voltage and current. It would seem a-priori contradictory to obtain lower densities when the radiative flux to the capillary walls is increased, since this radiative flux must be balanced by the enthalpy flux of the ablated products; however, one must take into account that as the radiative emission is enhanced, the steady-state plasma cannot be sustained at the given temperature with the similar or higher density. Thus, the equilibrium is reached at lower ion densities, leading to correspondingly lower values of pressure and Ohmic power. The impact is quite significant; according to Figure 4, the same pressure (10^7 Pa, or 100 atm) can be obtained for the same power, but the enhanced radiation case corresponds to a temperature of 8 eV, compared to 1.5 eV for the free-free emission only. While these results must be considered with extreme caution – given the very approximate model used so far – they indicate that an optimal regime for propulsive applications would be found in the (partially) optically-thin regime.

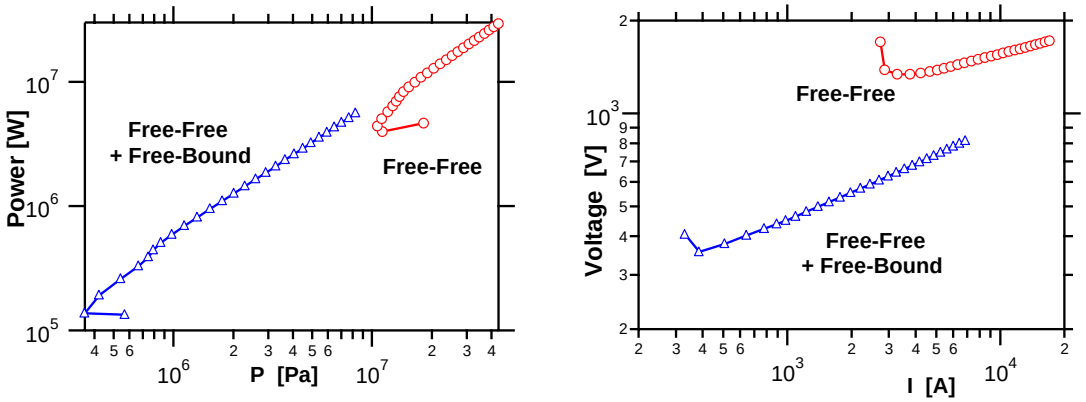

Figure 4: Impact of free-bound emission on key operating conditions for same range of temperature; free-free model is described by equation (13b), while equation (29) includes also free-bound emission.

The thermodynamic equilibrium model having been verified, it can be applied to the radiation models considered. One can make several observations from the results (including free-bound emission for the VR case), shown in Figure 5:

(1) The difference in pressure (and therefore plasma density) between the BB and VR models is up to 3 orders of magnitude; clearly, the VR case leads to conditions much more amenable to longer pulses, repeated use, and higher duty cycles.
(2) A similar observation can be made for the voltage supply (see Figure 5-d) and the current, both decreasing by at least an order of magnitude; this leads to reduced power dissipation and more compact circuit and pulse forming network.
(3) The deposited (Ohmic) power is also considerably reduced in the VR case, facilitating thermal management for high duty cycles.
(4) The mass flow rate is typically 1 kg/s f the BB case, leading to a recession rate of approximately 1 mm/s by ablation; in the VR case, the required mass flow is sufficiently small that liquid mass injection is possible, using a few % of the capillary wall area as injector area.

(5) As mentioned in the previous section, the BB model is barely valid (according to the Rosseland m.f.p.) at high temperature and pressure, while the VR model appears to be a consistent model throughout the explored conditions.

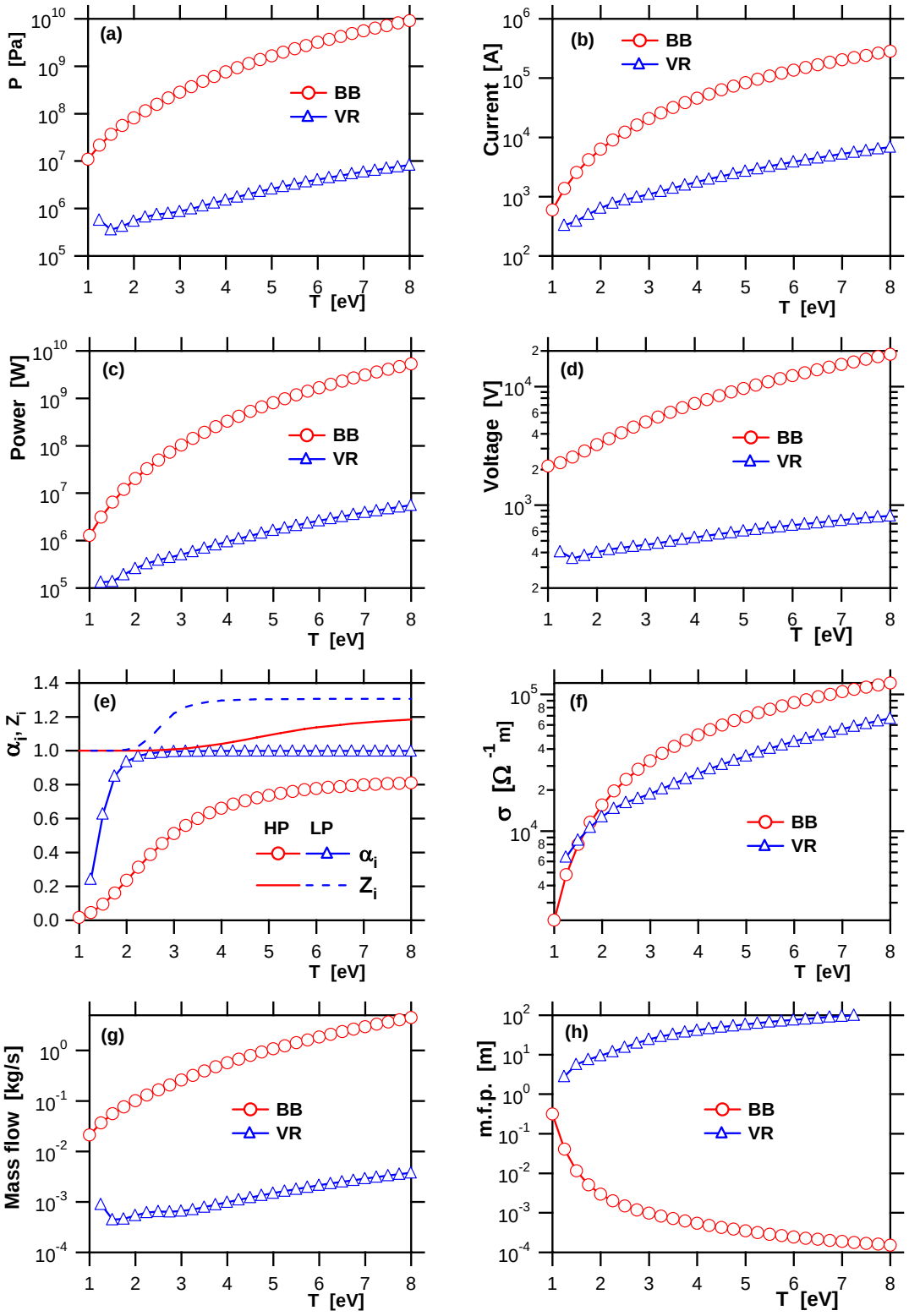

Figure 5: Plasma conditions for BB and VR (including free-bound) models, $L_c = 10\,\text{cm}$, $R_c = 2\,\text{mm}$, thermodynamic equilibrium computation.

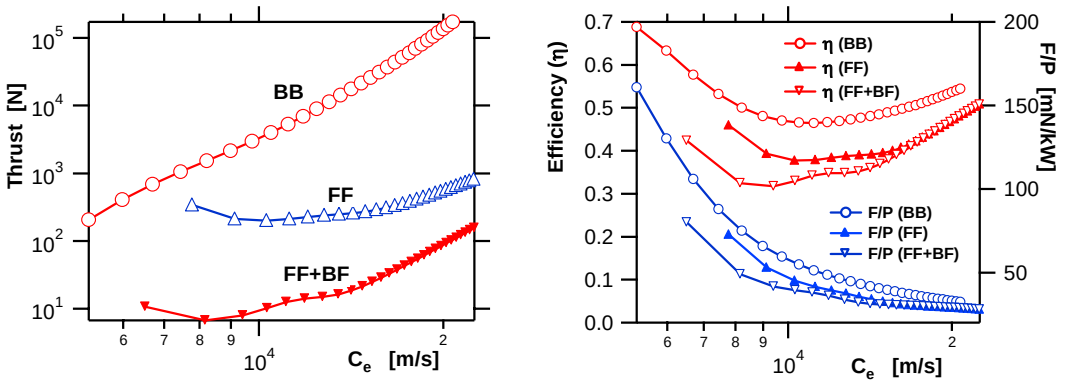

Figure 6: Left: comparison of thrust versus speed of sound at sonic point for the three radiation models, for single capillary of radius $R_c = 2\,\mathrm{mm}$, assuming steady-state; Right: propulsion efficiency (left axis) and thrust/power ratio, assuming expansion to Mach 3.

The prospects for propulsive applications can be evaluated from Figure 6, which show the potential thrust (assuming steady-state) that can be achieved by a single capillary of radius 2 mm. Steady-state operation, or at least high-duty cycle, being more realistically achieved in the engine volumetric radiation case, one can presume that a thrust of approximately 100 N per capillary would be obtained with a specific impulse (Isp) in excess of 2000 s; multiple capillaries could be bundled onto a single engine, and lower molecular weight propellants can be used to increase both figures of merit. Thus, the capillary discharge has the potential for simultaneously high-thrust and high-Isp propulsion, provided sufficient power is available. Also shown in Figure 6, propulsive efficiency (kinetic to electric power ratio) can be in the 40-50% range, comparable with a state-of-the-art EP thrusters (e.g. Hall-effect thruster - HET) and thrust-to-power ratio ranges between 30-100 mN/kW, also comparable to the HET and consistent with the 70 mN/kW quoted in Section 1 for the PET. Further model development and analysis is required before more definitive conclusions can be drawn. In particular, we plan to accomplish the following in the near-future:

- Implement a detailed radiation model with radiation transport
- Examine the unsteady equations and investigate stability conditions
- Include heat conduction into and within the solid walls

4 References

Burton R., Fleisher D., Goldstein S. & Tidman D. (1990) *AIAA J. Prop. & Power*, vol. **6**, 139.

Burton R.L. (1991) *IEEE Trans. Plasma Sci.*, vol. **19**, 340.

Cros B. et al. (2000) *IEEE Trans. Plasma Sci.*, vol. **28**, 1071.

Gilligan J. and Mohanti R. (1990) *IEEE Trans. Plasma Science*, vol. **18**, 190.

Griem R.H. (1962) *Phys. Rev.* **128**, 997.

Loeb A. and Kaplan Z. (1989), *IEEE Trans. Magnetics*, vol. **25**, 342.

Powell J. and Zielinski A. (1992),A. E., "Theory and Experiment for an Ablating Capillary Discharge and Application to Electrothermal-Chemical Guns", Army Ballistic Research Laboratory, Report BRL-TR-3355, June 1992.

Shafir N., Zoler D., Wald S. and Shapira M. (2005) *IEEE Trans. Magn.*, vol. **41**, 355.

Spitzer L. and Härm R. (1953) *Phys. Rev.*, vol. **89**, 977.

Tidman D, Thio Y., Goldstein S. and Spicer D. (1986) *GT-Devices report* 80-7

Zeldovich Ya. and Raizer Yu. (2002) *Physics of Shock Waves and High Temperature Hydrodynamic Phenomena*, 2nd-edition, Dover Publ. Inc, New-York.

Zoler D., Saphier D. and Alimi R. (1994) *J. Phys. D* vol. **27**, 142

Zoler D. and Alimi R. (1995) *J. Phys. D* vol. **28**, 1141.